



Experiments on the relationship between shape and effectiveness for three-dimensional boundary layer trips at supersonic speeds
by Stephen Edward Berger

A thesis submitted in partial fulfillment of the requirements for the degree of Master of Science in Mechanical Engineering
Montana State University
© Copyright by Stephen Edward Berger (1988)

Abstract:

Measurements to determine the effects of size and shape on the performance of three-dimensional boundary layer trips were made in the Montana State University Supersonic Wind Tunnel. Seventeen trips, representing four basic shapes, were examined. Experiments were conducted in the areas of Schlieren photography, drag force, wake turbulence, velocity profiles, and spanwise turbulent wake profiles behind paired trips. The results indicate that the planform shape and the forward rake angle of a trip have as much bearing on its effectiveness as the previously-known dependence on roughness height and frontal area. Trips of wedge planform were found to exhibit the best combination of desired performance characteristics. Standard trips were found to produce a previously undocumented, fully turbulent, distorted wake that bloomed away from the wall as the flow proceeded downstream. The spanwise wake influence of paired trips was not influenced by their relative spacing and orientation.

EXPERIMENTS ON THE RELATIONSHIP BETWEEN SHAPE AND
EFFECTIVENESS FOR THREE-DIMENSIONAL BOUNDARY
LAYER TRIPS AT SUPERSONIC SPEEDS

by

Stephen Edward Berger

A thesis submitted in partial fulfillment
of the requirements for the degree

of

Master of Science

in

Mechanical Engineering

MONTANA STATE UNIVERSITY
Bozeman, Montana

May 1988

N378
B4538

APPROVAL

of a thesis submitted by

Stephen Edward Berger

This thesis has been read by each member of the thesis committee and has been found to be satisfactory regarding content, English usage, format, citations, bibliographic style, and consistency, and is ready for submission to the College of Graduate Studies.

5/10/88
Date

Avenetradz
Chairperson, Graduate Committee

Approved for the Major Department

5-10-88
Date

Michael K. Hall
Head, Major Department

Approved for the College of Graduate Studies

5-13-88
Date

W. Malone
Graduate Dean

STATEMENT OF PERMISSION TO USE

In presenting this thesis in partial fulfillment of the requirements for a master's degree at Montana State University, I agree that the Library shall make it available to borrowers under rules of the Library. Brief quotations from this thesis are allowable without special permission, provided that accurate acknowledgement of source is made.

Permission for extensive quotation from or reproduction of this thesis may be granted by my major professor, or in his absence, by the Dean of Libraries when, in the opinion of either, the proposed use of the material is for scholarly purposes. Any copying or use of the materials in this thesis for financial gain shall not be allowed without my written permission.

Signature

Stephen E. Berger

Date

10 MAY 1988

ACKNOWLEDGMENTS

The author is indebted to the following persons for their contribution to this investigation.

His advisor, Anthony Demetriades, for his guidance and cooperation throughout the investigation.

Pat Vowell, for design input and expert construction of the special equipment used in the investigation.

John Rompel, for his assistance with the electronic laboratory equipment.

Alan H. George, for his advice on measurement techniques and instrumentation.

Thomas C. Reihman and William R. Martindale, for serving on the graduate committee and reviewing this thesis.

The Mechanical Engineering Department of Montana State University and AVCO Systems/Textron for financial assistance.

Rene' Tritz, for typing and checking the final version of this thesis.

TABLE OF CONTENTS

	Page
LIST OF TABLES	viii
LIST OF FIGURES	ix
NOMENCLATURE	xiv
ABSTRACT	xvii
1. INTRODUCTION	1
2. REVIEW OF PREVIOUS EXPERIMENTAL FINDINGS	4
Summary of Previous Findings	4
Implications for This Investigation	11
3. OUTLINE OF THE INVESTIGATION	13
Goals	13
Scope of the Investigation	13
Trips	14
Facilities and Equipment	15
Test Matrix	17
A Note on the Presentation of Test Data	18
4. TARE MEASUREMENTS	19
Experimental Apparatus and Procedures	19
Boundary Layer Properties	19
Turbulence Transition	20
Results	21
Boundary Layer Properties	21
Wall v. Floor Thickness	27
Turbulence Transition	28
5. PHOTOGRAPHIC INVESTIGATION OF TRIP PERFORMANCE	30
Experimental Apparatus and Procedures	30
Results	32
Calibration Photographs	32
Trip Photographs	32
Bow Shock Instability on Large, Blunt Trips ..	43

TABLE OF CONTENTS--Continued

	Page
6. DRAG FORCE MEASUREMENTS	46
Introduction	46
Experimental Apparatus and Procedures	46
Microbalances	46
Trip Installation	49
Installation in the SWT	50
Data Acquisition	52
Calibration	53
Results	59
Steady-State Drag	59
Measured v. Theoretical Drag	67
Unsteady drag	73
Trip Selection	76
7. TURBULENCE MEASUREMENTS	77
Introduction	77
Principle of Operation for the	
Dynamic Pressure Probe	79
Experimental Apparatus and Procedures	83
Dynamic Pressure Probe	83
Data Acquisition	84
Data Reduction	84
Tare Measurements	87
Results	88
DPP Failure	92
Trip Selection	92
8. BOUNDARY LAYER PROFILES	93
Introduction	93
Experimental Apparatus and Procedures	93
Results	95
9. WAKE TURBULENCE BEHIND PAIRED TRIPS	102
Introduction	102
Experimental Apparatus and Procedures	103
Results	105
10. CONCLUSIONS	112
REFERENCES CITED	115

TABLE OF CONTENTS--Continued

	Page
APPENDICES	119
Appendix A--Boundary Layer Profile	
Data Reduction Program	120
Appendix B--Microbalance Calibration	133
Appendix C--Dynamic Pressure Probe Calibration .	138
Appendix D--Comparison Between Trip Performance and the Potter-Whitfield Trip Sizing Correlation	145

LIST OF TABLES

Table	Page
1. Trip Identification and Dimensions (Dimensions in Centimeters)	14
2. Calculated v. Measured Drag for Selected Trips ...	72

LIST OF FIGURES

Figure	Page
1. Geometry and Nomenclature for Trip Construction	15
2. Major Components of MSU SWT (Reproduced from {12})	16
3. Laminar Boundary Layer Thickness on the SWT Floor and Wall	22
4. Laminar Boundary Layer Momentum Thickness on the SWT Floor and Wall	23
5. Laminar Boundary Layer Displacement Thickness on the SWT Floor and Wall	24
6. Unit Reynolds Number Distribution on the SWT Floor	25
7. Unit Reynolds Number Distribution on the SWT Sidewall	26
8. Mach Number Distribution in a Representative 2-Dimensional Laval Nozzle (from {16})	27
9. Onset and Completion of Transition to Turbulence in the MSU SWT	28
10. Method Used to Align Trips With the SWT Flow	31
11. Spark Photos of Tare Flow at $P_o = 620$ mm. Hg (top left) and 350 mm. Hg (top right). Continuous-Exposure Photo of Tare Flow at $P_o = 350$ mm. Hg (bottom right). Trip W-3 at Same position and Schlieren Settings, No Flow (bottom left)	33
12. Trip P-1 at Continuous (top) and Spark (bottom) exposure	34

LIST OF FIGURES--Continued

Figure	Page
13. Trips P-3 (left) and P-4 (right) Taken with Continuous (top) and Spark (bottom) Exposure	35
14. Trips W-1 (left) and W-2 (right) Taken with Continuous (top) and Spark (bottom) Exposure	36
15. Trips W-3 (left) and W-4 (right) Taken with Continuous (top) and Spark (bottom) Exposure	37
16. Trips S-1 (left) and S-2 (right) Taken with Continuous (top) and Spark (bottom) Exposure	38
17. Trips S-3 (left) and S-4 (right) Taken with Continuous (top) and Spark (bottom) Exposure	39
18. Trips S-5 (left) and S-6 (right) Taken with Continuous (top) and Spark (bottom) Exposure	40
19. Trips S-7 (left) and S-8 (right) Taken with Continuous (top) and Spark (bottom) Exposure	41
20. Continuous (top) and Spark (bottom) Photos of Trip STR-1	42
21. Evidence of Flow Instability over the S-5 Trip Observed with Spark Photography	44
22. Principal Components of the Microbalance	47
23. Methods of Trip Installation on the Microbalances	49
24. Trip S-2 Mounted on the 50-Gram Microbalance (left). Trip P-1 Mounted on the 10-Gram Microbalance (right)	50
25. Microbalance Orientation in the SWT Sidewall	51
26. Microbalance Data Acquisition Block Diagram	52
27. D.C. Signal v. Load for 4 Calibration Runs with the 50-Gram Microbalance	55
28. Tare A.C. and D.C. Outputs for the 50-Gram Microbalance (2 runs)	56

LIST OF FIGURES--Continued

Figure	Page
29. Typical Hysteresis Trace for the 50-Gram Microbalance (Trip S-3)	58
30. Typical Hysteresis Trace for the 10-Gram Microbalance (Trip P-4)	59
31. Drag Force v. Stagnation Pressure for Standard, Wedge and Strake Trips	60
32. Drag Force v. Stagnation Pressure for Low-Drag Trips	61
33. Drag/ P_o v. P_o for Standard, Wedge and Strake Trips	64
34. Drag/ P_o v. P_o for Low-Drag Trips	65
35. Drag Coefficient v. Re_δ for Large Standard Trips	68
36. Drag Coefficient v. Re_δ for Small Standard Trips	69
37. Drag Coefficient v. Re_δ for Wedge Trips	70
38. Drag Coefficient v. Re_δ for Thin Wedges and Plates	71
39. Unsteady Drag v. P_o for Three Standard Trips	74
40. Normalized Unsteady Drag v. P_o for Selected Trips	75
41. Sensitivity Coefficient v. Mach Number for Air ...	82
42. Major Features of the DPP Design	83
43. Block Diagram of the DPP Electronic Configuration	85
44. Block Diagram of the DPP Data Storage System	86
45. Analog Trace of the DPP A.C. Signal in a Turbulent Boundary Layer (2 runs)	89

LIST OF FIGURES--Continued

Figure	Page
46. Analog Trace of the DPP D.C. Signal in a Turbulent Boundary Layer (2 Runs)	89
47. DPP Frequency Spectra (Tare Measurements)	90
48. dU/U v. Y/Δ from DPP Data Plotted with Hot-Film Data from {21}	91
49. SWT Configuration for Boundary Layer Velocity Profiles	94
50. Normalized Boundary Layer Profile Behind W-1	96
51. Dimensional Boundary Layer Profile Behind Trip S-5	98
52. Normalized Boundary Layer Profile Behind trip S-5	99
53. Velocity Profile Map Behind Trip S-5 (Dashed Line is the Edge of the Turbulence)	100
54. Velocity Profile Map Behind Trip W-1	101
55. SWT Configuration for the Paired-Trip Experiments	103
56. Hot-Film RMS Signal Intensity v. Rotation Angle (2W Spacing)	106
57. Hot-Film RMS Signal Intensity v. Rotation Angle (3W Spacing)	107
58. Hot-Film Wake Traverses Behind a Single Trip	108
59. Turbulent Zone-Width Map at 0 and 90 degrees - 2W Spacing	110
60. Turbulent Zone-Width Map at 0 and 90 degrees - 3W Spacing	111
61. Boundary Layer Parameter Calculation Program	121
62. Configuration for Microbalance Calibration	134

LIST OF FIGURES--Continued

Figure	Page
63. DPP Signal v. Time for Varied Temperature Environments	139
64. DPP v. Standard Pitot Tube Profiles in a Laminar Boundary Layer	140
65. DPP v. Standard Pitot Tube Profiles in a Turbulent Boundary Layer	141
66. Calculated DPP Sensitivity for 11 Calibration Runs	143
67. Block Diagram of the DPP Improved Calibration Method	144
68. Trip Correlations with the Potter-Whitfield Performance Curve (Plotted on the Original graph from {5})	152

NOMENCLATURE

<u>Symbol</u>	<u>Description</u>
A	Frontal area of trip
A.C.	Alternating current
C_p	Constant pressure specific heat
C_d	Drag coefficient
D.C.	Direct current
DPP	Dynamic Pressure Probe
DVM	Digital voltmeter
F	Fahrenheit
F_d	Drag force
FFT	Fast Fourier transform
Gm	Gram
k	Roughness height
KHz	Kilocycles per second
L	Length of trip at the base
L'	Length of trip at the top
M	Mach number
M_t	Test section Mach number
mV	Millivolt
mG	Milligram
MSU	Montana State University

NOMENCLATURE--Continued

N	Noise level for A.C. signals
P	Pressure
PVC	Polyvinyl Chloride
R	Gas constant for air
Re	Reynolds number
Re'	Unit Reynolds number
Re' _k	Trip Reynolds number (Re')(k)
RMS	Root mean square
S	Sensitivity coefficient in chapter 7: Trip spacing in chapter 9
STK	Stock
SWT	Supersonic Wind Tunnel
T	Temperature
U	Free-stream velocity in X-direction
v.	Versus (in comparison to)
W	Width of trip
X	Streamwise coordinate axis
X _k	Trip location
Y	Coordinate axis normal to the wall
\tilde{Y}	Compressible transformed distance
Z	Spanwise coordinate axis
α	Half-angle
γ	Ratio of specific heats
δ	Boundary layer thickness

NOMENCLATURE--Continued

δ^*	Boundary layer displacement thickness
ϵ	Re'_k when $X_t = X_k$
θ	Boundary layer momentum thickness: Paired-trip orientation in chapter 9
ϕ	Rake angle of trip
ρ	Density
$d()$	Differential quantity
P-()	Plate trip-designator
S-()	Standard trip-designator
STR-()	Strake trip-designator
W-()	Wedge trip-designator
$()_{\delta}$, $()_e$	Property at the boundary layer edge
$()_k$	Property at $X = X_k$, $Y = k$ in a smooth-wall laminar boundary layer
$()_o$	Stagnation property
$()_t$	Property at the onset of transition: Property at the stagnation point of a pitot tube in chapter 7
$()_w$	Property at the base of the boundary layer (wall)
$()_{aw}$	Adiabatic-wall property
$()_{xk}$	Property at $X = X_k$
$()'$	RMS value of a property

ABSTRACT

Measurements to determine the effects of size and shape on the performance of three-dimensional boundary layer trips were made in the Montana State University Supersonic Wind Tunnel. Seventeen trips, representing four basic shapes, were examined. Experiments were conducted in the areas of Schlieren photography, drag force, wake turbulence, velocity profiles, and spanwise turbulent wake profiles behind paired trips. The results indicate that the planform shape and the forward rake angle of a trip have as much bearing on its effectiveness as the previously-known dependence on roughness height and frontal area. Trips of wedge planform were found to exhibit the best combination of desired performance characteristics. Standard trips were found to produce a previously undocumented, fully turbulent, distorted wake that bloomed away from the wall as the flow proceeded downstream. The spanwise wake influence of paired trips was not influenced by their relative spacing and orientation.

CHAPTER 1

INTRODUCTION

Methods of artificially forcing a laminar boundary layer to become turbulent are important both for designers of flight vehicles and for aerodynamic research. In flight vehicle design, it is often necessary to create a turbulent boundary layer ahead of engine inlets and control surfaces in order to prevent unwanted boundary layer separation. In research, particularly for high-speed flow experiments on scale models in wind tunnels (e.g., at Mach numbers greater than 10), it is often impossible to obtain any turbulence at all without resorting to artificial means.

The primary method for inducing turbulence in supersonic or hypersonic laminar boundary layers is by the use of individual protuberances, of roughness height (k) as tall as or taller than the laminar boundary layer thickness, distributed on the surface of a flight vehicle or scale model. Large protuberances are required because the temperature gradient in a high-speed, compressible boundary layer creates such low densities near the wall that low-height roughnesses, such as a band of grit or a

knurled surface, are totally ineffective as turbulence promoters. These large, three-dimensional protuberances, known as "trips", have been studied by numerous investigators for the purpose of optimizing their effectiveness, which is defined by the following criteria:

1. The onset of transition from laminar to turbulent flow should occur as close to the trip as possible, ideally at the trailing edge.
2. The trip should not substantially increase the total drag on the flight vehicle or scale model.
3. The effect of the trip should be confined to the boundary layer: it should not cause substantial distortion of the free-stream flowfield.
4. The turbulence induced by the trip should exhibit the same characteristics as natural (free flight) turbulence at a reasonable distance downstream of the trip. Specifically: the velocity profile, heat transfer characteristics, boundary layer thickness, momentum thickness, and displacement thickness of the trip-induced boundary layer should be similar to those found in a naturally-turbulent boundary layer. This requirement is especially critical in wind tunnel experiments.

Despite the extensive amount of research on the performance of trips, little work has been done on the relationship between trip geometry and trip effectiveness. An investigation was therefore undertaken for the purpose of determining the effect of trip geometry on trip effectiveness in supersonic flow.

CHAPTER 2

REVIEW OF PREVIOUS EXPERIMENTAL FINDINGS

Summary of Previous Findings

Due to the lack of a definitive theory on the performance of three-dimensional protuberances in supersonic boundary layers, the bulk of the useful work on the subject of trip effectiveness has been experimental.

Typical of research on trips in low-speed flow is the work of Klebanoff and Tidstrom (1) who, in a study of transition behind a two-dimensional trip, concluded that tripped transition is a stability-governed phenomenon. Specifically, disturbances which are unstable according to the laminar boundary-layer stability theory are greatly amplified within a "recovery zone" (defined as the region in the area downstream of the trip where the mean flow is distorted by the presence of the trip itself). That is, the apparent action of the trip is to create a destabilizing influence on the flow in the recovery zone so that existing (i.e., not trip-induced) unstable disturbances are amplified faster than the natural (untripped) rate. These investigators also found

that transition behind two-dimensional tripping elements changes gradually as the free-stream unit Reynolds number is increased, but transition behind a three-dimensional element changes suddenly when the unit Reynolds number reaches a critical value.

Experimentation on trip effectiveness at supersonic and hypersonic speeds began in the 1950s. Van Driest and McCauley (2), in an experiment using spherical tripping elements on a 5-degree half-angle cone at Mach 1.9 and 3.67, concluded that the horseshoe vortex generated by the tripping element is the mechanism that creates early transition. The horseshoe vortex is said to "contaminate and break down the surrounding vorticity field". Transition was observed to move close to the trip location "suddenly" at a critical trip Reynolds number Re_k , defined as $((Re')_\delta)(k)$, where δ is the smooth-wall boundary layer thickness at X_k . The critical trip Reynolds number also corresponded to the lowest transition Reynolds number in all cases presented. The critical trip Reynolds number was found to be proportional to $Re_{xk}^{1/4}$, where Re_{xk} is the free stream smooth-wall Reynolds number at the trip location. The 1/4-power relationship was shown to be valid for different trip heights, trip locations, and edge Mach numbers. The significance of these findings is that,

given the flow parameters, the trip location, and the proportionality constant, it should be possible to determine k such that the critical, or 'effective' trip Reynolds number criterion is met and transition occurs at the lowest possible local Reynolds number. Lateral trip spacing was found to have little effect on the location of the onset of transition, as long as the lateral separation was large enough to prevent interference between the horseshoe vortices behind each trip throughout the transition zone. Additionally, the vortex strength was found to persist in the laminar sublayer of the turbulent boundary layer after transition.

Van Driest and Blumer (3) extended the findings of Reference (2) to include the effects of heat transfer and the values of the proportionality constant for flat plates and cones. The relationship is given as:

$$k/X_k = 33.4 \left[1 + .9 \left(\frac{T_w}{T_{aw}} - 1 \right) + .28 \left(\frac{T_{aw}}{T_\delta} - 1 \right) \right] Re_{xk}^{-3/4}$$

For flat plates, the proportionality constant is 44.0.

Whitehead (4), in a study of flowfield and drag characteristics of various tripping elements in a Mach 6.8 flow over a flat plate, also noted the horseshoe-vortex phenomena seen by Van Driest and McCauley. Although Whitehead's observations were presented qualitatively

(the primary goal of the experiment was to determine the effect of trip size and shape on drag), he specifically noted that lateral trip spacing had little or no influence on trip effectiveness as long as the spacing was greater than 3 trip widths. Regarding drag, Whitehead observed that the extent of boundary-layer separation at the leading edge influences trip-induced drag at constant trip height and width. Additionally, he found that the relationship between trip-induced drag and trip height becomes constant above about $k = 2\delta$ for cylindrical and wedge-shaped trips, but not for spherical trips. An incidental finding in this paper is that the horseshoe vortex appears to vanish ahead of the wedge-planform trip (it does not appear in the oil-stain photographs).

Potter and Whitfield (5), in an experiment on tripped flows on the exterior of a sharp-lipped tube at hypersonic Mach numbers, found that disturbances in the boundary layer ahead of the trip (which lead to early transition) may arise from the trip bow shock/boundary layer interaction, with free-stream turbulence as a forcing parameter. They noted that the transition process behind large trips can produce distortions in the flow outside the natural boundary layer which persist well downstream of the trip location. These undesirable side-effects result in flow characteristics that do not simulate natural turbulence

and, if too severe, may defeat the purpose of the trip. These investigators also found that three-dimensional elements are more effective than two-dimensional elements in hypersonic flow (2-d elements become less and less effective at increasing Mach numbers). Even so, the minimum trip height required to move the onset of transition to the trip location was found to increase exponentially with the Mach number.

The major contribution of this paper is the development of an empirical correlation between trip location (X_k), trip height (k), desired location of transition onset behind the trip (X_t), location of transition on the smooth (untripped) surface (X_{t0}), and a "disturbance parameter" (Re'_k/ϵ). The Potter-Whitfield correlation can be used in principle to determine the trip size required to locate transition anywhere between the trip position and the location of smooth-wall transition.

Pate {6}, in an experiment on flow over a 5-degree half-angle cone at Mach 3 and 4, investigated the effect of free-stream disturbances on tripped transition by performing the same series of experiments in two different wind tunnels. The purpose of his investigation was to determine whether or not the differences in free-stream disturbances that exist in different wind tunnels would invalidate the Van Driest-Blumer or Potter-Whitfield

correlations. Pate concluded that the absolute location of transition behind a given trip in a given flow was definitely influenced by the free-stream disturbance level. However, the correlations of Potter-Whitfield and Van Driest-Blumer were shown to remain valid. An additional and important finding was that the performance of different trips relative to each other remained unchanged.

An investigation by Nestler and McCauley {7} had a similar conclusion as that of Potter and Whitfield regarding the bow shock-boundary layer interaction as the generator of early transition, at least in the case of large, bluff trips. Unlike other investigators, however, they found that lateral spacing has a maximum critical value as well as having a minimum critical value. These investigators used multiple rows of cube-shaped trips in their experiments and found that the Van Driest-Blumer correlation (which was developed for a single row of spherical trips) was reasonably valid for some other combinations of trip shape, trip size, trip spacing, and nose bluntness.

Strike {8} performed a series of experiments on spherical and serrated tripping elements over a 6-degree half-angle cone at hypersonic {Mach 8} speeds. He concluded that three staggered rows of spherical trips are as effective in causing early transition as a single row with

twice the roughness height. This discovery is important in that many of the undesirable effects of trips on the flowfield are caused by excess roughness height. He also found that staggered rows of trips provide better lateral uniformity in the downstream heat transfer and flow properties, that large trips create upstream influences on the heat transfer and pressure properties, and that flowfield disturbances persist for a much greater distance downstream of a single row of large trips than behind staggered rows of smaller trips.

Whitfield and Iannuzzi {9} conducted experiments on a 4.5 degree half-angle cone at very high Mach numbers (14 to 16) and found that the roughness height required for effective tripping increased exponentially with the Mach number (see Potter and Whitfield above). They postulated that the use of very large trips (in an attempt to move transition forward at high Mach numbers) may be self-defeating. That is to say, large trips distort the flowfield so severely that it may not be possible to trip the boundary layer at hypersonic Mach numbers without unacceptable distortion.

McCauley, Saydah and Bleuche {10} measured the flow over a 6-degree half-angle cone at Mach 10 and a Re' of 1.6×10^6 /ft, using spherical trips and varying both the angle of attack and the wall temperature. The results of

their experiments confirmed the Van Driest-Blumer correlation (but with a different proportionality constant) under hypersonic conditions.

Implications for This Investigation

The findings of the investigators cited above were used to establish the scope of the present investigation. The implications of previous work in the field of trip effectiveness, and the application of these findings to the present investigation, can be summarized as follows:

1. The fact that three-dimensional trips are much more effective than two-dimensional trips in supersonic and hypersonic flows is well-established. Therefore, experiments on two-dimensional trips can be dismissed out of hand in the present investigation.
2. The performance of spherical trips has been exhaustively investigated and documented. It would therefore serve no purpose to experiment on spherical trips in the present investigation.
3. Despite the fact that many of the trips in actual use are of rectangular planform and frontal profile (referred to as "standard" trips in this investigation), the data on the effectiveness of trips of other than spherical shape is very sparse. It is safe to say that the optimum trip shape for effective

tripping action has not been determined. Therefore, a study of the relationship between trip shape and trip effectiveness has the best potential for contributing to the body of knowledge on this topic.

4. Most of the data contained in previous experiments was derived from surface measurements, or by means of single-point hot-wire anemometry. A need therefore exists for obtaining continuous data throughout the boundary layer, particularly in regard to velocity and turbulence profiles.

CHAPTER 3

OUTLINE OF THE INVESTIGATION

Goals

The primary goal of this investigation was to determine the relative effect of different trip shapes on trip effectiveness, with the aim of determining the "best" shape. An equally important goal was to determine the best roughness height (k) for the trip or trips of "best" shape, in the hope that this roughness height would be smaller than that of a spherical or a standard trip of equivalent performance.

Scope of the Investigation

During the design of the investigation, it was determined that all the aspects of trip effectiveness listed in Chapter 1 should be explored. Therefore, experiments were devised for the measurement of drag force, turbulence intensity, and flowfield disturbance behind each of the trips in the investigation. An additional experiment was performed on the effect of trip spacing and orientation on trip effectiveness. Recently, experiments in a hypersonic (Mach 8) wind tunnel on the

effectiveness of some of the trips in this study have become available for comparison (Reference {11}).

Trips

The trips used in the investigation are listed in Table 1. The trips fall into four categories: strakes; flat plates; wedges; and standard trips. Nomenclature used to describe trip features is as shown in Figure 1.

Table 1. Trip Identification and Dimensions
(Dimensions in Centimeters)

Trip No.	k	L	L'	ϕ (deg.)	α (deg.)	W
Plates:						
P-1	1.25	1.25	0.75	45.0		
P-2	1.25	1.25	1.25	90.0		
P-3	0.25	1.75	1.75	90.0		
P-4	1.25	0.75	0.75	90.0		
Wedges:						
W-1	0.50	1.25	0.75	90.0	17.0	
W-2	0.50	1.25	0.25	90.0	5.7	
W-3	1.25	1.25	0.75	90.0	17.0	
W-4	1.25	0.75	1.25	90.0	9.5	
Standard Trips:						
S-1	0.75	3.75	0.95	15.0		0.75
S-2	0.75	2.00	0.70	30.0		0.75
S-3	0.25	1.25	0.31	15.0		0.75
S-4	1.25	0.50	0.33	15.0		0.75
S-5	0.90	1.60	1.08	60.0		0.90
S-6	0.90	1.60	1.36	75.0		0.90
S-7	0.90	1.50	0.00	30.0		0.95
S-8	0.30	1.50	1.33	60.0		0.90
Strakes:						
STR-1	1.00	1.90	0.00	27.76	14.74	1.00

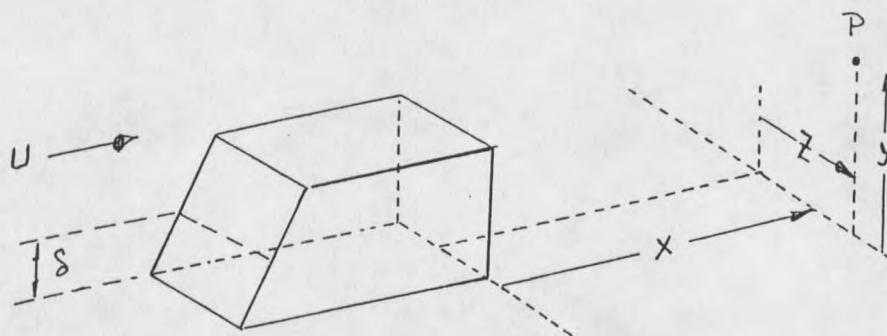
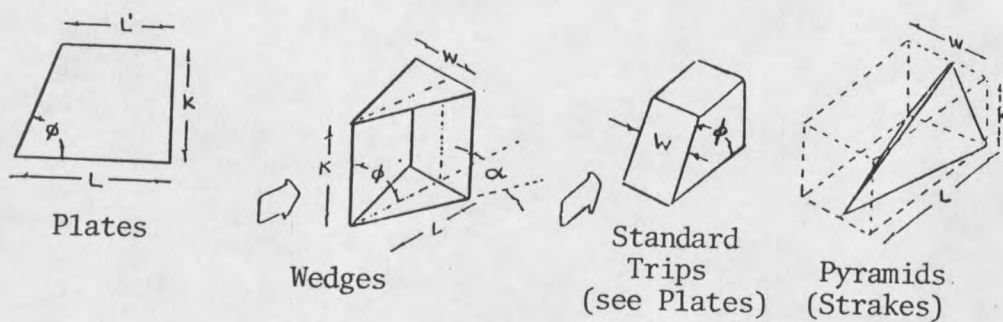


Figure 1. Geometry and Nomenclature for Trip Construction

The trips were constructed from Lexan or PVC plastic, the material having been chosen for its ease of machineability and its suitability for operation at the temperatures encountered in the MSU SWT.

Facilities and Equipment

All of the experiments in the test matrix were performed in the MSU Supersonic Wind Tunnel (SWT). The SWT is an open-circuit, continuous-flow facility, using

air as the working fluid and producing a nominal test section Mach number of 3.0 over a Re' range of 580,000 to 1.7 million per inch. Figure 2 illustrates the main features of the SWT, which is fully described in Reference {12}.

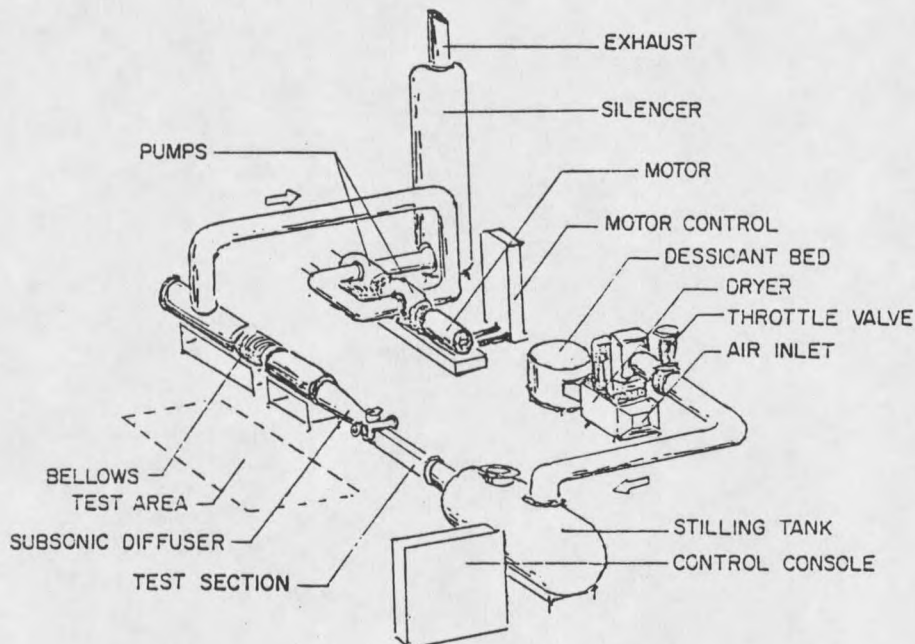


Figure 2. Major Components of MSU SWT
(Reproduced from {12})

General-purpose data acquisition for the test matrix was obtained by the use of the SWT Automated Data Acquisition System. The system, which provides probe control and data capture capability for SWT operations, was redesigned specifically for this investigation.

A complete description of the Data Acquisition System is found in Reference {13}.

In addition to the general-purpose equipment listed above, a number of sensors and devices were custom-built for this investigation. These are described in the chapters corresponding to their application.

Test Matrix

Due to the comprehensive nature of this investigation, and the large number of trips to be examined, it was determined early in the planning stage that all of the trips could not be examined for all aspects of trip performance. The test matrix was therefore organized so as to "screen out" a portion of the test group in each stage of the investigation. The early stages of the matrix were purely qualitative, thereby providing rapid means to perform the screening-out procedure. The later stages were used to obtain data more amenable to quantitative analysis, but only on the best-performing trips.

The test matrix was constructed as follows:

1. Tare measurements performed for the purpose of obtaining laminar boundary layer properties and transition data required in subsequent stages.

2. Photographic studies of the boundary layer downstream of each trip in the test series by means of the SWT Schlieren system.
3. Drag force measurements on each trip in the test series, using a purpose-built load sensor.
4. Quantitative turbulence measurements in the boundary layer downstream of the "best" trips, as determined by the results of items 2 and 3 above, using an experimental Dynamic Pressure Probe (DPP).
5. Flow-velocity studies (boundary layer profiles) downstream of the trips not screened out after stages 3 and 4, using a pitot tube and the Automated Data Acquisition System.
6. Turbulence profiles in the wake of paired trips, to determine the effects of trip spacing and orientation on turbulence generation.

A Note on Presentation of the Test Data

In order to preserve the continuity of presentation, the experimental procedures and the results for each stage in the test matrix are described in separate chapters.

CHAPTER 4

TARE MEASUREMENTS

Experimental Apparatus and ProceduresBoundary Layer Properties

Laminar and turbulent boundary layer measurements were made at the centerline of the SWT nozzle surface ("floor") and at the centerline of the sidewall ("wall"), using a .004 in. diameter pitot tube. These measurements were taken for the purpose of establishing the streamwise rate of growth of Re' , δ , δ^* , and θ , under laminar and turbulent conditions, for use in later stages of the test matrix. Full boundary layer profiles were also taken for comparison with trip-induced profiles generated later in the test matrix.

The floor data were taken over the range $X = 8.64$ in. to $X = 18.64$ in. (X measured downstream from the nozzle throat) at 1/2 in. intervals. The wall data were taken at 1 in. intervals from $X = 11.14$ in. to $X = 18.14$ in. Data runs were made at $P_0 = 350$ mm. Hg (laminar) and at $P_0 = 600$ mm. Hg (turbulent). T_0 was 100° F for all data runs.

Measurements were made by traversing the pitot tube from the surface (wall or floor) to a point well past the edge of the boundary layer, in .004 in. increments. The data points were captured by an earlier version of the SWT Automated Data Acquisition System (functionally similar to the system described in {13}), and reduced to useable form by means of the computer program listed in Appendix A.

Turbulence Transition

Measurements were taken to establish the stagnation pressure (P_0) at which turbulence first appears at a given X-station in the SWT. These measurements were used for positioning trips, in later stages of the test matrix, at locations of known laminar flow in the smooth-wall boundary layer. The data were also required to establish the stagnation conditions which provide the longest run of laminar flow in the SWT.

The transition data were taken by setting a hot-film anemometer in the boundary layer at a given X-station and observing its RMS A.C. signal as the SWT P_0 was swept. The total temperature (T_0) was maintained at 100° F. The anemometer signal indicates the level of velocity and density fluctuation (turbulence), and can thus be used to detect both the onset and the completion of turbulence transition.

Results

Boundary Layer Properties

Variations of the laminar ($P_0 = 350$ mm. Hg) boundary layer edge properties δ , θ , and δ^* , as functions of the X-station are shown in Figures 3 through 5. The wall data points in each of these figures exhibit considerable scatter, which is attributed to excess motion of the pitot probe due to mechanical problems with the SWT Z-Axis actuator.

Included in the figures are simple correlations for the variation of the edge properties in the downstream direction. These correlations were used for calculations in later stages of the test matrix.

Figures 6 and 7 are plots of the variation in Re' in the streamwise direction, on the floor and wall respectively. The data in these plots, consistent with previous measurements made in the SWT (see {12}), were considered valid for the purposes of this investigation.

